Active Elastic Metamaterials for Zero-Frequency and Zero-Wavenumber Bandgaps

Brahim Lemkalli,[1] Alaa M. Ali,[1] Qingxiang Ji,[1,*] Julio Andrés Iglesias Martínez,[2]
Younes Achaoui,[3] Sebastien Guenneau,[4] Richard Craster,[4] and Muamer Kadic[1]

[1] *Université Marie et Louis Pasteur, Institut FEMTO-ST, CNRS UMR 6174, Besançon, 25000, France*
[2] *Université de Lorraine, Institut Jean Lamour, CNRS UMR 7198, Nancy 54000, France*
[3] *OPTIMEE Laboratory, Department of Physics, Moulay Ismail University, B.P. 11201, Zitoune, Meknes, Morocco*
[4] *UMI 2004 Abraham de Moivre-CNRS, Imperial College London, SW7 2AZ, London, UK*

We create wave-matter stimuli responsive metamaterials using optical trapping forces to manipulate mass-spring chains and create zero-frequency and zero-wavenumber band gaps: the bosonic nature of phonons, and hence this elastodynamic setting, traditionally prohibits either zero-frequency or zero-wavenumber band gaps. Here, we generate zero-frequency gaps using optomechanical interactions within a 3D mass-spring chain by applying an optical trapping force to hold or manipulate a mass in a contactless manner independent of its elastodynamic excitations. Through careful modification of the geometrical parameters in the trapped monoatomic mass-spring chain, we demonstrate the existence of a zero-frequency gap generated by the optical forces on the masses. The precise control we have over the system allows us to drive another set of masses and springs out of phase with its traveling wave thereby creating a zero-wavenumber band gap.

I. INTRODUCTION

For centuries, researchers have focused on how acoustic and electromagnetic waves interact with matter to better understand material properties and govern wave propagation; these investigations are critical for a variety of applications, ranging from understanding the origins of the universe to developing new devices and technology. The field of photon-matter interaction, which studies how electromagnetic waves interact with matter, has grown beyond its initial boundaries and now involves the application of mechanical stress on matter via the energy, linear momentum, and angular momentum of light. Historically, Johannes Kepler was the first to identify this phenomenon in 1619 by observing the deflection of comet tails by sunlight, thereby establishing that light can exert mechanical forces on matter [1]. Building on this concept, Arthur Ashkin introduced the application of optical forces in 1970, leading to the development of optical tweezers [2–4]. The use of light for trapping microparticles has since led to groundbreaking discoveries and diverse applications in fields such as chemistry [5–7], nanotechnology [8–11], quantum science [12], plasmonics [13], thermodynamics [14], and microrobotics [15–18].
In parallel, the field has also transformed into a dynamic exploration of phonon vibrations within phononic crystals and metamaterials [19–22]. This research aims to generate stop band gaps, which are generally essential for a variety of applications, such as shielding [23–25], sensing [26–29], and filtering [30, 31]. In this context, Benchabane et *al.* demonstrated the control of surface acoustic waves using shallow and cylindrical pillars on piezoelectric plates, aiming to enable wave filtering and sensing through phononic crystals [32–36]. Inspired by photonic crystals, phononic structures control the propagation of phonons using an array of periodic scatterers and create high-frequency band gaps via Bragg scattering, with the periodic constant matching the wavelength of the incident wave [37–40]. Notably, creating low-frequency band gaps with periodic arrays of scatterers was challenging. However, in 2000, the concept of local resonance emerged, revolutionizing band gap creation by introducing a mechanism where propagating modes interact with locally resonant modes, resulting in low-frequency local band gaps [41]. Following this, metamaterials with sub-wavelength band gaps arose, owing to the aforementioned mechanisms. Since then, substantial optimization has permitted the development of low-frequency band gaps in many acoustic applications [42, 43].

Exploiting bandgaps at near-zero frequencies allows for precise control of wave fields, with potential applications in managing low-frequency mechanical waves for seismic, and sound control; the zero-frequency bandgap is named for its forbidden zone starting at zero frequency. It was first studied in the context of the quasi-static approximation of the acoustic band [44] and low frequency plasmons [45] in metallic photonic crystals. The key fundamental aspect of obtaining a zero-frequency bandgap for phonons is to get either zero stiffness over a range of frequencies starting from zero (which is forbidden by the thermodynamic laws) or to have an infinite mass density (forbidden by the standard model). Most studies on zero-frequency bandgaps have sidestepped this by using clamped holes or pillars with Dirichlet boundary conditions. Theoretical studies on pinned plates have examined the existence of zero-frequency stop-bands to shield elastic waves using clamped holes arranged in square arrays with Dirichlet conditions [46]. Another study explored generating a zero-frequency bandgap using clamped pillars embedded in bedrock based on fixed pillars [47]. More recently, a Bragg gap at nearly zero frequency has been proposed by introducing an additional degree of freedom represented by spin motion, which interacts with the longitudinal motion of a mass in a diatomic mechanical system [48].

* qingxiang.ji@femto-st.fr

In this work, we propose a novel paradigm for creating either zero-frequency and zero-wavenumber stop band gaps through optomechanical interactions. Employing highly focused laser beams, formed with aspherical lenses that act as optical tweezers, we effectively trap masses within optical potentials. In such traps, optical forces contribute additional mechanical forces to the masses, akin to supplemental springs attached to each mass. Furthermore, due to the higher propagation velocities of optical waves compared to elastic waves, optical forces can be applied significantly faster than any comparable acoustic counterpart. This allows for the creation of highly responsive, controllable systems in the spirit of space-time metamaterials, where optical forces can be dynamically activated. This phenomenon of optomechanical trapping results in the emergence of zero-frequency bandgaps when the effective optical stiffness is positive, and zero-wavenumber bandgaps when it is effectively negative. More intriguingly, using this same type of optical actuation, we have been able to mimic negative springs by modulating the optical traps, resulting in a zero-wavenumber bandgap.

II. COMPUTATIONAL METHODS

Our optomechanical model, as shown in Fig. 1(a), is constructed as a monoatomic mass-spring chain, and each mass is exposed to optical forces generated by a highly focused laser beam by aspherical lenses with a numerical aperture N.A.= 1.29 and made up of a material with the refractive index of $n = 1.52$: this laser-focused beam, with a wavelength of 1064nm, acts as a local optical tweezer. In the trapping condition, the mass acts as if it is attached to another spring, depending on the optical stiffness, which is represented by the equivalent model at the top of Fig. 1(a). The geometrical parameters of the mass-spring elementary cell are illustrated in Fig. 1(b), in which the periodic lattice constant has a constant of $a = 5$ μm and spherical masses with a radius of $r = 1.5$ μm. For the mechanical calculations reported here we use polymer-like material with material density $\rho = 1100$ kg/m^3, Young's modulus of 1 GPa for masses and 2.7 MPa for springs, and Poisson's ratio $\nu = 0.4$.

Firstly, we calculate the optical forces exerted on the masses to verify their practicability and potential experimental verification. We consider a circular polarization for the incident wave with the parameters mentioned earlier, and the plane wave becomes focused due to the aspherical lens and creates a Gaussian-like beam. The distribution of the electric field on the mass-spring unit cell is depicted in Fig. 1(c). The result is obtained by simulations performed in COMSOL Multiphysics 6.2. In this figure, we have a full view of the mass and a cross-section in the xz-plane for an incident wave propagating upward in the z-direction. Using the outcomes of this simulation, we calculate the trapping efficiencies as a function of the positions x, y, and z in the mass: $Q_i = cF_i/n_{\text{air}}P$ with

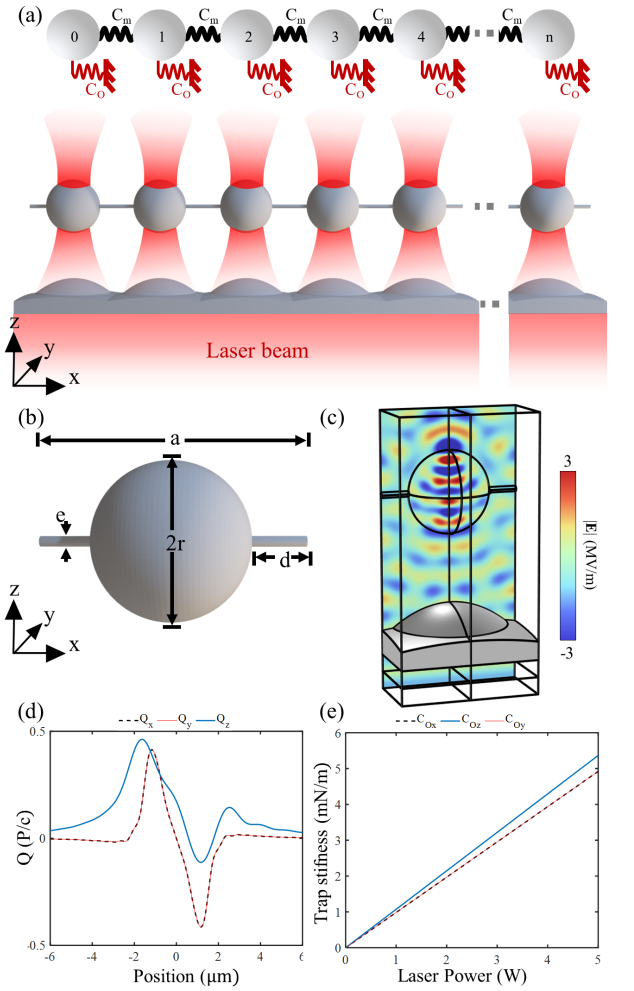

Fig. 1. Principle of an optomechanically controlled monoatomic mass-spring chain. (a) Illustration of the spherical masses arranged as a monoatomic toy model connected via C_m springs and the optical trapping stiffness C_O acting on each mass as being attached to the foundation. The lower panel shows the corresponding physically realizable mechanical system composed of spherical masses connected by rods and illuminated via an optical metasurface composed of spherical-like lenses acting individually as traps on the spheres. A linearly polarized optical laser is illuminating the system from the bottom (in the z-direction) (b) The geometric representation of the unit cell with a periodicity constant $a = 5$ μm, the mass radius $r = 1.5$ μm, the length of the cylinder $d = 1$ μm and the diameter $e = 0.2$ μm. (c) An illustration of the distribution of the electric field modulus imposed on the spherical mass by the focused laser beam. (d) The trapping efficiencies (Q_x, Q_y, Q_z) for the sphere immersed, are graphed in the transverse x, y (black dotted and red lines respectively) and longitudinal z (black line) directions, as function of the particle displacement from the nominal paraxial focus. (e) The equivalent optical stiffness in the function of the laser power along the 3 principal directions.

$i = x$, y, or z, c is the light velocity, P is the laser power, n_{air} is the refractive index of air, and F_i is the optical forces (see Appendix A); the results of the normalized trapping efficiencies are illustrated in Fig. 1(d).

At the equilibrium point, the optical force can be linearized as an elastic restoring force with a negative slope, e.g., $F_x = -C_{Ox}x$ for the x-direction. Thus, optical forces can be approximated with an effective harmonic potential with spring constants or trap stiffnesses C_{Ox}, C_{Oy}, and C_{Oz}. To calculate the optical trap's stiffness, we simply get the slope of the force-displacement graphs at the equilibrium position, where the force vanishes. In Fig. 1(e), we show the calculated stiffness as a function of laser power. The optical analysis is conducted in COMSOL Multiphysics 6.2.

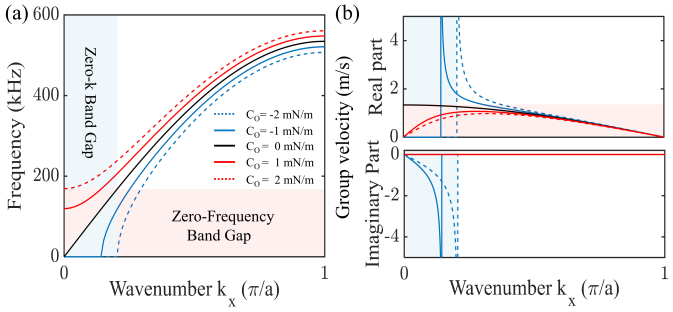

Fig. 2. (a) Analytical phononic dispersion curves in the first irreducible Brillouin zone along x-direction as a function of the stiffness of the optical traps C_O on the mass-spring model, with $C_m = 0.01$ N/m, $a = 5$ μm, and the Bloch wavenumber $k_x \in [0, \pi/a]$. (b) Corresponding real and imaginary parts of the group velocity $v_g = \frac{d\omega}{dk}$ are depicted versus wavenumber k_x.

Secondly, we derive the dispersion relation for the mass-spring chain by starting with an analytical model where optical mass trapping is equated to a monoatomic mass-spring system. In this model, each mass is subjected to a highly focused laser that exerts Maxwell stress in the z-direction. This setup is analogous to a classical mechanical system where a mass is attached to an additional spring, with the spring's stiffness determined by the optical forces applied by the laser trap. Fig. 1(a) illustrates the optical trapping mechanism and its equivalent model for n masses.

To calculate the dispersion diagrams, we analyze the motion of the masses in the system mentioned before. By extracting the forces applied to each mass in the chain, we write the Lagrangian for the mechanical system, which consists of n masses connected by springs with a spring constant C_m, and each mass attached to a clamping spring with stiffness $C_O = C_{Ox}$ depending on the optical force applied to that mass. The Lagrangian is expressed as follows:

$$L = \tfrac{1}{2}\sum_{i=0}^{n}\left[m\dot{u}_i^2 + C_m\left(\left(u_{i+1}-u_i\right)^2 - \left(u_i - u_{i-1}\right)^2\right) - C_o u_i^2\right], \quad (1)$$

where u_i is the displacement of mass m_i from its equilibrium position, $\dot{u}_i$ its time derivative, m is the mass of each particle in the chain (assuming all masses are identical), C_m is the spring constant of the springs connecting each mass to its neighbors, u_{i-1} and u_{i+1} are the displacements of the neighboring masses, and C_O is the spring constant describing the optical force.

To solve this system of equations, we need to derive the Lagrangian equation for each degree of freedom, as follows: $\frac{d}{dt}\left(\frac{dL}{d\dot{u}_i}\right) - \frac{\partial L}{\partial u_i} = 0$. In addition, we assume Bloch waves in the system, as follows:

$$u_i(t) = U_i e^{j(nk_x a - \omega t)}, \quad (2)$$

where $\mathrm{j}^2 = -1$, U_i $(i = 1, \cdots, \mathrm{n})$ is the amplitude of u_i, k_x the component of the wavevector $\mathbf{k}$ along x, a the pitch of the array and ω the angular frequency.

Solving these equations (see Appendix B), we obtain the dispersion relation of the system:

$$\omega = \sqrt{\frac{2}{m}\left(C_m \sin^2\left(\frac{k_x a}{2}\right) + C_O\right)}. \quad (3)$$

III. RESULTS AND DISCUSSION

A. Infinite trapped mass-spring model

In Fig. 2, we plot the analytical dispersion of the longitudinal wave of the monatomic mass-spring system, where each mass is connected to an optical stiffness C_O. We depict the phononic dispersion along an edge of the first irreducible Brillouin zone (ΓX), where $\Gamma = (0, 0, 0)$ and $X = (\pi/a, 0, 0)$, assuming that the cells are repeated periodically along the x-direction and finite in the yz-plane, making use of the rotational symmetry of the spheres and beams, and aware of dangers of using edges of the Brillouin zone [49]. The first mode, represented in a black line, begins at zero frequency and has an optical stiffness constant set to zero. This shows typical dispersion without a zero-frequency band gap. In other words, the group velocity is not zero; therefore, any wave polarization travels through the mass-spring system. This behavior is typical of a system in which wave propagation is dependent on the material properties, allowing all waves to pass through the medium. However, when an optical stiffness of 1 mN/m is added to the mass, as indicated by the red line curve, a zero-frequency band gap appears. This indicates that the group velocity equals zero at these frequencies, forbidding wave propagation over the zero-stop-band gap. As a result, no wave will pass through the system at these frequencies, demonstrating the presence of a zero bandgap caused by the additional optical springs. This shows that applying forces equivalent to a constant spring stiffness introduces a zero-frequency band gap. Further, when additional forces are applied to the mass, such as in the red dotted line curve where

C_O is 2 mN/m, the zero-frequency band gap becomes larger, and the longitudinal mode at $k_x = 0$ shifts to higher frequencies. This is an analytical demonstration that applying optical forces to the masses results in the formation of a zero-frequency band gap in a monoatomic mass-spring chain.

Another remarkable phenomenon occurs when the stiffness of one of the optical forces becomes negative, specifically reaching values of -1 mN/m and -2 mN/m in the case of the black dotted line and line curves, respectively. This negative stiffness induces the formation of a zero-wavenumber band gap. In this band gap, the group velocity, which describes the speed at which elastic waves propagate through the mass-spring system, diverges to infinity. This means that within this band gap, the wave packets associated with the optical forces can theoretically travel instantaneously, leading to unique and potentially useful physical properties.

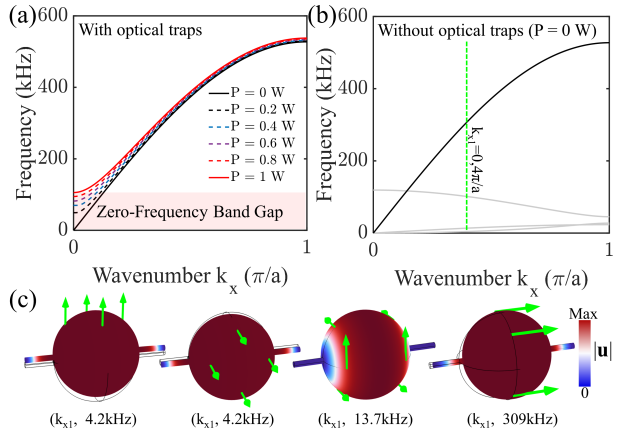

Fig. 3. Phononic dispersion curves in the first irreducible Brillouin zone ΓX for infinite structure. (a) The dispersion curves without optical traps. The longitudinal mode is highlighted in black, while the other modes are shown in gray. (b) The evolution of the longitudinal mode as a function of laser power. The stronger the Laser power P, the wider the zero-frequency stop band. (c) Screenshots of the eigenmodes at $k_{x1} = 0.4\pi/a$ display the four fundamental modes: two degenerate transverse modes, a torsional mode, and a longitudinal mode, respectively.

After calculating the analytical phononic dispersion in the first Brillouin zone along the x-direction, we numerically calculate its counterpart using the Finite Element Method (FEM) using the elementary cell shown in Fig. 1(b), taking into account the optical stiffness calculated for several values of the laser power up to 1 W (see Appendix C).

Fig. 3 depicts the results of eigenvalue calculations. Several major conclusions can be drawn from this figure: at zero frequency, there is no longitudinal mode, indicating that any longitudinally polarized elastic wave cannot propagate at these near-zero frequencies.

Furthermore, we conduct a sweep calculation of the eigenfrequencies of each mode as a function of the laser power; the results of this investigation are illustrated in Fig. 3(a). As the power of the laser increases, the upper range of the zero-frequency band gap of each mode shifts to a higher frequency; the frequency range of the zero-gap is controlled by the altered laser power.

B. Finite trapped mass-spring model

Until now, we have demonstrated the existence of the zero-frequency and zero-wavenumber band gaps in an infinite array of a monoatomic mass-spring chain. Now, we proceed to calculate the phononic diagrams and demonstrate the existence of the zero-gaps in the case of a finite array composed of $n = 40$ elementary cells, which is an experimental approach to demonstrate the existence of the zero-frequency band gap. The schematic illustration of this array is presented in Fig. 1(a) with $n = 40$. We take into account the optical stiffness applied to each mass by the highly focused laser beam. We use the time domain study to solve the problem, by exciting the finite array with a noise signal, and at each of the $i = 0, 1, \ldots, 39$ masses we evaluate the displacement amplitude $|U_{x,y,\text{ or }z}(t)|$ over real-time t. Then we conduct the 2D Fast Fourier Transformation from time-real space to frequency-wavenumber, and we obtain 40 points within the first Brillouin zone $k_x \in [-\pi/a, \pi/a]$. To ensure consistency across frequencies, we normalize the displacement amplitude to a unity power density such that $\sum_{i=0}^{39} |U_i(k_x, \omega)|^2 = 1$. Furthermore, to better understand the zero gap, we calculate the transmission between the fast Fourier transformation of the displacements at the first mass ($i = 0$) and the last mass ($i = 39$), by using the expression for the transmission, T, as $\mathrm{T} = 20 \log_{10}\left(\frac{|U_{39}(\omega)|}{|U_0(\omega)|}\right)$.

Fig. 4 presents the calculated band structures for the infinite array of mass-spring chains within the first Brillouin zone and its calculated transmission over the frequency. The phononic dispersion results presented in Fig. 4(a) are displayed on false-color scales, additionally, black solid curves represent band structure calculations for an infinitely periodic array along the y-direction.

In the phononic dispersion, we plot three fundamental modes: bending and transverse modes and longitudinal mode. One can see that all modes have zero frequency band gaps, which is demonstrated by the transmission calculation in Fig. 4(b), in which the transmission still equals -47 dB along the $0 - 80$ kHz frequency range.

Lastly, we now actively trap and move the previously explained traps in order to control, like in space-time metamaterials, the applied stiffness on the masses. Doing it in this configuration, we can make a counteracting spring leading to a negative stiffness. The corresponding dispersion relation is given in Fig. 5. We see a clear signature of a zero wave number region from 0 to a finite wave number where no possible mode could be excited to fit a

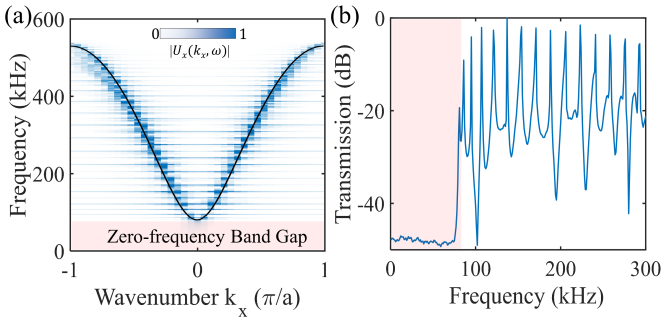

Fig. 4. Finite mass-spring chain optically trapped in the temporal domain. (a) The calculated phononic dispersion of a finite mass-spring chain under optical traps for 40 unit cells along the x-axis. The modulus $|U_x(k_x, \omega)|$ of the complex response function is plotted on a false-color scale versus the x-component k_x of the wave vector and frequency $f = \omega/2\pi$. The black solid line represents the numerical computation of dispersion for an infinite mass-spring chain. (b) The calculated transmission in dB between the modulus of the input x-component displacement and the modulus of the output after 40 unit cells x-component displacement.

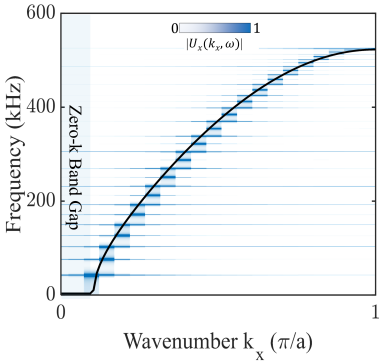

Fig. 5. Finite mass-spring chain optically driven in the temporal domain. The calculated phononic dispersion of a finite mass-spring chain under optical traps for 40 unit cells along the x-axis.

small wavenumber (i.e. large wavelength). We mention in passing that all the mentioned dispersion calculations are performed in COMSOL Multiphysics 6.2.

IV. CONCLUSION

In conclusion, we present an approach that uses optical tweezers to trap and precisely manipulate masses in mass-spring arrays, creating a zero-frequency band gap and also a zero-wavenumber gap. This study introduces an experimental paradigm for generating these band gaps via optomechanical interactions, offering an alternative to conventional methods that use clamped pillars or holes in the zero-frequency case. A challenge for time-varying metamaterials, where the time period of the material modulation is desired to be similar, or less, than that of the wavelength is to modulate a material fast enough; in optics this requires femtosecond modulation pushing the boundaries of experimental laser physics [50]. The technique used here in the simple mechanical system, using local optical tweezers, allows effective manipulation of matter on timescales much shorter than the waves in the chain: this opens the way to validating theoretical results for time-modulated metamaterials.

ACKNOWLEDGEMENTS

The authors acknowledge the support of the ANR PNanoBot project (contract "ANR-21-CE33-0015"), Marie Skłodowska-Curie Actions Postdoctoral Fellowships [No. 101149710] and National Natural Science Foundation of China [Nos. 12302169]. This paper is part of a special issue dedicated to our colleague and friend Dr Sarah Benchabanne, a pioneer in surface acoustic wave (SAW) phononics [32–34, 51] and in phoxonics [52, 53].

[1] J. D. Jackson, Electrodynamics, classical, in *digital Encyclopedia of Applied Physics* (John Wiley & Sons, Ltd, 2003).

[2] A. Ashkin, Acceleration and trapping of particles by radiation pressure, Phys. Rev. Lett. **24**, 156 (1970).

[3] A. Ashkin, Atomic-beam deflection by resonance-radiation pressure, Phys. Rev. Lett. **25**, 1321 (1970).

[4] A. Ashkin, J. M. Dziedzic, J. E. Bjorkholm, and S. Chu, Observation of a single-beam gradient force optical trap for dielectric particles, Opt. Lett. **11**, 288 (1986).

[5] R. C. Sullivan, H. Boyer-Chelmo, K. Gorkowski, and H. Beydoun, Aerosol optical tweezers elucidate the chemistry, acidity, phase separations, and morphology of atmospheric microdroplets, Acc. Chem. Res. **53**, 2498 (2020).

[6] Y. Shen, D. A. Weitz, N. R. Forde, and M. Shayegan, Line optical tweezers as controllable micromachines: techniques and emerging trends, Soft Matter **18**, 5359 (2022).

[7] A. Zaltron, M. Merano, G. Mistura, C. Sada, and F. Seno, Optical tweezers in single-molecule experiments, Eur. Phys. J. Plus **135**, 896 (2020).

[8] O. M. Maragò, P. H. Jones, P. G. Gucciardi, G. Volpe, and A. C. Ferrari, Optical trapping and manipulation of nanostructures, Nat. Nanotechnol. **8**, 807—819 (2013).

[9] J. Melzer and E. McLeod, English (US)Assembly of multicomponent structures from hundreds of micron-scale building blocks using optical tweezers, Microsyst. Nanoeng. **7** (2021).

[10] E. Mcleod and C. B. Arnold, Array-based optical nanolithography using optically trapped microlenses., Opt. Express **17 5**, 3640 (2009).

[11] E. Mcleod and C. B. Arnold, Subwavelength direct-write nanopatterning using optically trapped microspheres., Nat. Nanotechnol. **3 7**, 413 (2008).

[12] A. Kaufman and K.-K. Ni, Quantum science with optical tweezer arrays of ultracold atoms and molecules, Nat. Phys. (2021).

[13] Y. Zhang, C. Min, X. Dou, X. Wang, H. P. Urbach, M. G. Somekh, and X. Yuan, Plasmonic tweezers: for nanoscale optical trapping and beyond, Light Sci. Appl. **10**, 59 (2021).

[14] J. Gieseler and J. Millen, Levitated nanoparticles for microscopic thermodynamics—a review, Entropy **20**, 10.3390/e20050326 (2018).

[15] E. Gerena, F. Legendre, A. Molawade, Y. Vitry, S. Régnier, and S. Haliyo, Tele–robotic platform for dexterous optical single-cell manipulation, Micromachines **10** (2019).

[16] D. Zhang, A. Barbot, B. Lo, and G.-Z. Yang, Distributed force control for microrobot manipulation via planar multi-spot optical tweezer, Adv. Opt. Mater. **8**, 2000543 (2020).

[17] Q. Ji, J. Moughames, X. Chen, G. Fang, J. J. Huaroto, V. Laude, J. A. I. Martínez, G. Ulliac, C. Clévy, P. Lutz, *et al.*, 4d thermomechanical metamaterials for soft microrobotics, Commun. Mater. **2**, 93 (2021).

[18] A. M. Ali, E. Gerena, J. A. I. Martínez, G. Ulliac, B. Lemkalli, A. Mohand-Ousaid, S. Haliyo, A. Bolopion, and M. Kadic, Optical chiral microrobot for out-of-plane rotation, Commun. Phys. **8**, 230 (2025).

[19] R. V. Craster, S. R. Guenneau, K. Muamer, and M. Wegener, Mechanical metamaterials, Rep. Prog. Phys. (2023).

[20] M. Kadic, G. W. Milton, M. van Hecke, and M. Wegener, 3d metamaterials, Nat. Rev. Phys. **1**, 198 (2019).

[21] B. Lemkalli, K. K. Dudek, M. Kadic, Q. Ji, S. Guenneau, A. Mir, and Y. Achaoui, W-shaped broadband attenuation of longitudinal waves through composite elastic metamaterial, Compos. Part B Eng. **297**, 112250 (2025).

[22] Y. Chen, M. Kadic, S. Guenneau, and M. Wegener, Isotropic chiral acoustic phonons in 3d quasicrystalline metamaterials, Phys. Rev. Lett. **124**, 235502 (2020).

[23] M. Miniaci, A. Krushynska, F. Bosia, and N. M. Pugno, Large scale mechanical metamaterials as seismic shields, New J. Phys. **18**, 083041 (2016).

[24] B. Lemkalli, S. Guenneau, Y. E. Badri, M. Kadic, H. Mangach, A. Mir, and Y. Achaoui, Seismic waves shielding using spherical matryoshka-like metamaterials, in *The Proceedings of the International Conference on Smart City Applications* (Springer, 2023) pp. 77–85.

[25] Y. M. Luo, C. He, Z. Tao, J. Hao, H. H. Xu, Y. Zhang, F. Zhang, and X. Ren, A surface-wave seismic metamaterial filled with auxetic foam, Int. J. Mech. Sci. , 108715 (2023).

[26] Z. Alrowaili, H. M. Fathy, H. A. Elsayed, M. Aouassa, M. Mahmoud, K. S. El-Nasser, T. Taha, and A. Mehaney, Heavy metals biosensor based on defective one-dimensional phononic crystals, Ultrasonics **130**, 106928 (2023).

[27] A. H. Almawgani, H. M. Fathy, H. A. Elsayed, G. A. Ali, M. Irfan, and A. Mehaney, Periodic and quasi-periodic one-dimensional phononic crystal biosensor: a comprehensive study for optimum sensor design, RSC Adv. **13**, 11967 (2023).

[28] R. Lucklum, M. Ke, and M. Zubtsov, Two-dimensional phononic crystal sensor based on a cavity mode, Sens. Actuators B Chem. **171**, 271 (2012).

[29] B. Lemkalli, M. Kadic, Y. El Badri, S. Guenneau, A. Mir, and Y. Achaoui, The emergence of low-frequency dual fano resonances in chiral twisting metamaterials, Wave Motion **127**, 103302 (2024).

[30] Y. Pennec, B. Djafari-Rouhani, J. O. Vasseur, A. Khelif, and P. A. Deymier, Tunable filtering and demultiplexing in phononic crystals with hollow cylinders, Phys. Rev. E **69**, 046608 (2004).

[31] Z. G. Chen, J. Zhao, J. Mei, and Y. Wu, Acoustic frequency filter based on anisotropic topological phononic crystals, Sci. Rep. **7**, 15005 (2017).

[32] S. Benchabane, O. Gaiffe, R. Salut, G. Ulliac, V. Laude, and K. Kokkonen, Guidance of surface waves in a micron-scale phononic crystal line-defect waveguide, Appl. Phys. Lett. **106** (2015).

[33] S. Benchabane, R. Salut, O. Gaiffe, V. Soumann, M. Addouche, V. Laude, and A. Khelif, Surface-wave coupling to single phononic subwavelength resonators, Phys. Rev. Appl. **8**, 034016 (2017).

[34] S. Benchabane, O. Gaiffe, G. Ulliac, R. Salut, Y. Achaoui, and V. Laude, Observation of surface-guided waves in holey hypersonic phononic crystal, Appl. Phys. Lett. **98** (2011).

[35] S. Benchabane, A. Jallouli, L. Raguin, O. Gaiffe, J. Chatellier, V. Soumann, J.-M. Cote, R. Salut, and A. Khelif, Nonlinear coupling of phononic resonators induced by surface acoustic waves, Phys. Rev. Appl. **16**, 054024 (2021).
[36] M. F. Groß, J. L. G. Schneider, Y. Wei, Y. Chen, S. Kalt, M. Kadic, X. Liu, G. Hu, and M. Wegener, Tetramode metamaterials as phonon polarizers, Adv. Mater. **35**, 2211801 (2023).
[37] M. Kushwaha and P. Halevi, Band-gap engineering in periodic elastic composites, Appl. Phys. Lett. **64**, 1085 (1994).
[38] B. Lemkalli, M. Kadic, Y. El Badri, S. Guenneau, A. Mir, and Y. Achaoui, Longitudinal-twist wave converter based on chiral metamaterials, New J. Phys. **26**, 073026 (2024).
[39] B. Lemkalli, O. T. Tugut, Q. Ji, R. Craster, S. Guenneau, M. Kadic, C. Bizzaglia, and B. Ungureanu, Controlling the propagation of flexural elastic waves with ceramic metatiles, Int. J. Mech. Sci. , 110520 (2025).
[40] F. M. De Espinosa, E. Jimenez, and M. Torres, Ultrasonic band gap in a periodic two-dimensional composite, Phys. Rev. Lett. **80**, 1208 (1998).
[41] Z. Liu, X. Zhang, Y. Mao, Y. Zhu, Z. Yang, C. T. Chan, and P. Sheng, Locally resonant sonic materials, science **289**, 1734 (2000).
[42] S. Brûlé, E. Javelaud, S. Enoch, and S. Guenneau, Experiments on seismic metamaterials: molding surface waves, Phys. Rev. Lett. **112**, 133901 (2014).
[43] N. Jiménez, V. Romero-García, V. Pagneux, and J.-P. Groby, Rainbow-trapping absorbers: Broadband, perfect and asymmetric sound absorption by subwavelength panels for transmission problems, Sci. Rep. **7**, 13595 (2017).
[44] N. Nicorovici, R. McPhedran, and L. Botten, Photonic band gaps: Noncommuting limits and the "acoustic band", Phys. Rev. Lett. **75**, 1507 (1995).
[45] J. B. Pendry, A. Holden, W. Stewart, and I. Youngs, Extremely low frequency plasmons in metallic mesostructures, Phys. Rev. Lett. **76**, 4773 (1996).
[46] T. Antonakakis, R. V. Craster, and S. Guenneau, Moulding and shielding flexural waves in elastic plates, EPL **105**, 54004 (2014).
[47] Y. Achaoui, T. Antonakakis, S. Brûlé, R. Craster, S. Enoch, and S. Guenneau, Clamped seismic metamaterials: ultra-low frequency stop bands, New J. Phys. **19**, 063022 (2017).
[48] J. H. Oh, S. J. Choi, J. K. Lee, and Y. Y. Kim, Zero-frequency bragg gap by spin-harnessed metamaterial, New J. Phys. **20**, 083035 (2018).
[49] R. Craster, T. Antonakakis, M. Makwana, and S. Guenneau, Dangers of using the edges of the brillouin zone, Phys. Rev. B **86**, 115130 (2012).
[50] R. Tirole, S. Vezzoli, E. Galiffi, I. Robertson, D. Maurice, B. Tilmann, S. A. Maier, J. B. Pendry, and R. Sapienza, Double-slit time diffraction at optical frequencies, Nat. Phys. **19**, 999 (2023).
[51] W. Wang, M. Baranski, Y. Jin, R. Salut, D. Belharet, J.-M. Friedt, Y. Pan, Y. Xiang, F.-z. Xuan, A. Khelif, *et al.*, Experimental realization of on-chip surface acoustic wave metasurfaces at sub-ghz, Adv. Sci. **12**, 2411825 (2025).
[52] V. Laude, J.-C. Beugnot, S. Benchabane, Y. Pennec, B. Djafari-Rouhani, N. Papanikolaou, J. M. Escalante, and A. Martinez, Simultaneous guidance of slow photons and slow acoustic phonons in silicon phoxonic crystal slabs, Opt. Express **19**, 9690 (2011).
[53] S. Benchabane, S. Sadat-Saleh, M.-P. Bernal, J.-C. Beugnot, V. Laude, Y. Pennec, B. Djafari-Rouhani, N. Papanikolaou, and A. Martinez, Phoxonic crystals: A review, in *Phononics 2011* (2011) p. 84.
[54] N. Malagnino, G. Pesce, A. Sasso, and E. Arimondo, Measurements of trapping efficiency and stiffness in optical tweezers, Opt. Commun. **214**, 15 (2002).
[55] P. Polimeno, A. Magazzu, M. A. Iati, F. Patti, R. Saija, C. D. E. Boschi, M. G. Donato, P. G. Gucciardi, P. H. Jones, G. Volpe, *et al.*, Optical tweezers and their applications, J. Quant. Spectrosc. Radiat. Transfer **218**, 131 (2018).

Appendix A: Mechanisms of optical trapping

In this section, we simplify optomechanical interaction by taking into account the orders of magnitude of the different frequencies related to the problem of optical oscillation against mass-spring vibrations. For the optical part, we consider a tweezer trap based on a laser operating at a wavelength of $\lambda = 1064$ nm, which corresponds to a frequency of 3×10^{14} Hz. For the acoustical problem, it is limited to frequencies within the MHz range due to the lattice constant of 5 μm. As a consequence, we could solve the electromagnetic problem independently and apply the outcome as a constant trapping force in the acoustic problem. The highly focused laser beam used in this work is like Gaussian with circular polarization, and its electric field can be expressed as follows:

$$\mathbf{E} = \mathbf{E}_0 \frac{w_0}{w(z)} \exp\left[-\frac{x^2+y^2}{w^2(z)} - jqz - jq\frac{x^2+y^2}{2R(z)} + j\eta(z)\right], \tag{A1}$$

where $j^2 = -1$, $\mathbf{E}_0 = E_0(1, j, 0)^T$, w_0 is the beam waist which is the radius at the focus, p_0 is the position of the focal plane which is zero in our case, q is the optical wavenumber, $w(z)$ is the radius at specific z position, and it is calculated as:

$$w(z) = w_0\sqrt{1 + \left(\frac{z-p_0}{z_0}\right)^2}, \tag{A2}$$

where $z_0 = \frac{qw_0^2}{2}$ and $R(z)$ is the radius of curvature of the beam's wavefront, and it is computed as:

$$R(z) = (z-p_0)\left[1 + \left(\frac{z_0}{z-p_0}\right)^2\right], \tag{A3}$$

$\eta(z)$ is the Gouy phase which is defined as a phase advance to the beam around the focal point which results in an increase in the wavelength near the waist; therefore, the phase velocity exceeds the speed of light. The Gouy phase is calculated according to equation A4:

$$\eta(z) = \tan^{-1}\left(\frac{z-p_0}{z_0}\right) \tag{A4}$$

The radiation pressure is then calculated using Maxwell's stress tensor, a parameter depending on the electric and magnetic field components of the total field (incident and scattered).

Generally, the stress is a 2nd-rank symmetric tensor depicted as:

$$\mathbf{T} = \begin{bmatrix} T_{xx} & T_{xy} & T_{xz} \\ T_{xy} & T_{yy} & T_{yz} \\ T_{xz} & T_{yz} & T_{zz} \end{bmatrix} \tag{A5}$$

Each component of this tensor can be computed from the previous field's components:

$$\begin{cases} T_{xx} = \Re[\epsilon_0(E_x E_x^* - \frac{1}{2}E^2) + \frac{1}{\mu_0}(B_x B_x^* - \frac{1}{2}B^2)] \\ T_{yy} = \Re[\epsilon_0(E_y E_y^* - \frac{1}{2}E^2) + \frac{1}{\mu_0}(B_y B_y^* - \frac{1}{2}B^2)] \\ T_{zz} = \Re[\epsilon_0(E_z E_z^* - \frac{1}{2}E^2) + \frac{1}{\mu_0}(B_z B_z^* - \frac{1}{2}B^2)] \\ T_{xy} = \Re[\epsilon_0(E_x E_y^*) + \frac{1}{\mu_0}(B_x B_y^*)] \\ T_{xz} = \Re[\epsilon_0(E_x E_z^*) + \frac{1}{\mu_0}(B_x B_z^*)] \\ T_{yz} = \Re[\epsilon_0(E_y E_z^*) + \frac{1}{\mu_0}(B_y B_z^*)] \end{cases} \tag{A6}$$

where $B^2 := \mathbf{B} \cdot \mathbf{B}^*$ and $E^2 := \mathbf{E} \cdot \mathbf{E}^*$.

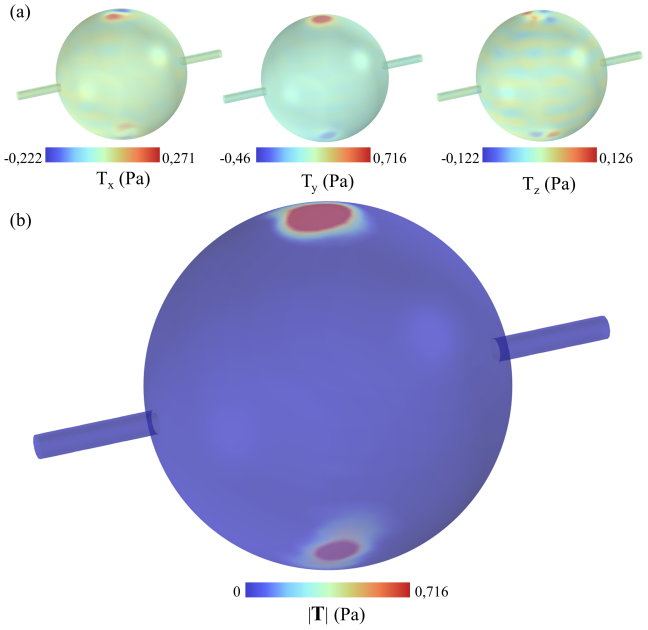

Fig. 6. Maxwell stress tensor distribution calculated by using an optical lens that focuses the laser beam on the mass-spring system. (a) The Maxwell stress tensor's x, y, and z-components. (b) The Maxwell Stress Tensor's modulus.

The total optical force is computed on a particle by integrating the stresses over the external surface using the equation $\mathbf{F} = \iint_S \mathbf{T} \cdot d\mathbf{S}$.

The theoretical description of optical forces depends on the comparison between the spherical mass radius r and the Gaussian laser wavelength λ. Optical trapping can be described in three main regimes based on whether the particle size is smaller than, comparable to, or larger than the wavelength. In our case, with a laser wavelength λ of 1 μm and a mass radius of approximately 1.5 μm, the particle size is significantly larger than the wavelength. Therefore, we use the geometrical optics approximation.

According to ray-optics theory, the maximum restoring radial or axial force occurs when the sphere is displaced from the focal point by a distance equal to its radius. Specifically, for the transverse force along the r-direction, the force is given by [54, 55]:

$$F = -C_{Or} r, \tag{A7}$$

Where r is x or y. Similarly, for the axial force along the z-direction, the force is given by:

$$F = -C_{Oz} r \tag{A8}$$

Here, C_{Or} and C_{Oz} are the radial and axial stiffness coefficients of the trap, respectively. The main relationship between the trapping force (axial or radial) and the laser power is:

$$F = \frac{Q_i n P}{c}, \tag{A9}$$

where Q_i is a dimensionless parameter that describes the radial and axial efficiency of the trap, representing the fraction of the laser beam's momentum $\frac{nP}{c}$ that is converted into the trapping force, for air the refractive index is equal to $n = 1$. The expressions of optical stiffness then follow from A7, A8 and A9:

$$\begin{aligned} C_{Ox} &= -\frac{Q_x}{r}\frac{P}{c}, \\ C_{Oy} &= -\frac{Q_y}{r}\frac{P}{c}, \\ C_{Oz} &= -\frac{Q_z}{r}\frac{P}{c} \end{aligned} \tag{A10}$$

Appendix B: Analytical phononic dispersion calculations

In this section, we detail the derivation of the analytical dispersion relation for the mass-spring chain where optical mass trapping is equated to a monoatomic mass-spring system. In this model, each mass is subjected to a highly focused laser that exerts Maxwell stress in the y-direction. This setup is analogous to a classical mechanical system where a mass is attached to an additional spring, with the spring's stiffness determined by the optical forces applied by the laser trap.

To compute the dispersion diagrams, we analyze the motion of the masses in the aforementioned system. By extracting the forces applied to each mass in the chain, we can write the Lagrangian for the mechanical system, which consists of n masses connected by springs with a

spring constant C_m, and each mass attached to a clamping spring with stiffness C_O depending on the optical force applied to that mass. The Lagrangian is expressed with 1.

To solve this system of equations, we need to derive the Lagrangian equation for each degree of freedom, as follows: $\frac{d}{dt}\left(\frac{dL}{d\dot{u}_i}\right) - \frac{\partial L}{\partial u_i} = 0$. Then, for each mass m_i in the chain, the equation of motion can be expressed as:

$$\begin{cases} m\ddot{u}_0 = C_m(u_1 + u_{-1} - 2u_0) - C_O u_0 \\ m\ddot{u}_1 = C_m(u_2 + u_0 - 2u_1) - C_O u_1 \\ \vdots \\ m\ddot{u}_n = C_m(u_{n+1} + u_{n-1} - 2u_n) - C_O u_n \end{cases}. \quad \text{(B1)}$$

The monoatomic chain is periodic with the lattice constant a, representing the distance between two nearest masses. Solutions of the system of equations (B1) are in the form of Bloch waves:

$$u_i(t) = U_i e^{j(nk_x a - \omega t)}, \quad \text{(B2)}$$

with U_i the amplitude, k_x the component of the wavevector $\mathbf{k}$ along x, and ω the angular frequency. The differential equations, along with these boundary conditions, fully describe the dynamics of the system of masses connected by springs in the infinite chain.

Solving these equations would provide the analytical solution for the displacement u_i of each mass in the chain as a function of wavenumber. Plugging the plane wave solution (B2) into the equation of motion (B1) results in the following system of equations:

$$\begin{cases} -\omega^2 m U_0 = C_m(U_1 e^{jk_x a} + U_{-1} e^{-jk_x a} - 2U_0) - C_O U_0 \\ -\omega^2 m U_1 = C_m(U_2 e^{jk_x a} + U_0 e^{-jk_x a} - 2U_1) - C_O U_1 \\ \vdots \\ -\omega^2 m U_n = C_m(U_{n+1} e^{jk_x a} + U_{n-1} e^{-jk_x a} - 2U_n) - C_O U_n \end{cases} \quad \text{(B3)}$$

which is nothing but an eigenvalue problem $C(k_x)\mathbf{U} = \omega^2 M\mathbf{U}$, where $\mathbf{U}$ is the amplitude vector, M the mass matrix ($M_{ij,i=j} = m$), and $C(k_x)$ a stiffness matrix denoted as follows:

$$C(k_x) = \begin{bmatrix} 2C_m + C_O & -C_m e^{jk_x a} & 0 & \dots & 0 \\ -C_m e^{-jk_x a} & 2C_m + C_O & -C e^{jk_x a} & \dots & 0 \\ 0 & -C_m e^{-ik_x a} & 2C_m + C_O & \dots & 0 \\ \vdots & \vdots & \vdots & \ddots & \vdots \\ 0 & 0 & 0 & \dots & 2C_m + C_O \end{bmatrix} \quad \text{(B4)}$$

To compute the dispersion curves arising from (B3), we look for roots of the determinant $\det(\mathrm{C(k_x)} - \omega^2 \mathrm{M}) = 0$.

To streamline the calculation of the system of equations (B3), we selected two nearest neighbor masses i and $i+1$, respectively. Then, we compute the dispersion of the longitudinal mode by using the expression derived from (B3) as a function of the optical stiffness constant that describes the optical forces applied to both masses, as illustrated by the equation 3.

Appendix C: Infinite numerical phononic dispersion calculation methods

In this section, we use the commercial software COMSOL multiphysics to numerically solve the eigenvalue equation derived from Cauchy elasticity, using a similar system to the one studied in the analytical model, by considering an infinite monoatomic mass-spring chain composed of spherical masses with a radius r and n springs attached to these masses with stiffness C_m. In order to enhance optical trapping in finite element simulations, we use spring foundation boundaries to apply the calculated optical forces to each mass. Then, we solve the elasticity equation starting with the equilibrium equations.

$$\nabla \cdot \boldsymbol{\sigma} + \mathbf{b} = \mathbf{0} \quad \text{(C1)}$$

Combined with the Caushy elastic equation (Generalized Hooke's Law):

$$\boldsymbol{\sigma} = \mathbf{C} : \boldsymbol{\varepsilon}. \quad \text{(C2)}$$

where the strain-displacement relation:

$$\boldsymbol{\varepsilon} = \frac{1}{2}\left(\nabla \mathbf{u} + (\nabla \mathbf{u})^T\right). \quad \text{(C3)}$$

where $\boldsymbol{\sigma}$ is the stress tensor, $\mathbf{b}$ is the body force vector, $\mathbf{C}$ is the elasticity tensor, $\boldsymbol{\varepsilon}$ is the strain tensor, and $\mathbf{u}$ is the displacement vector.

Substituting equation (C3) into Cauchy elasticity for an isotropic homogeneous linear material, leads to the eigenvalue problem:

$$-\rho\omega^2 \mathbf{u} = \frac{E}{2(1+\nu)(1-2\nu)} \nabla\nabla \cdot \mathbf{u} + \frac{E}{2(1+\nu)} \nabla^2 \mathbf{u} \quad \text{(C4)}$$

with E the Young's modulus, ν the Poisson's ratio, ρ the density, ω the angular frequency, and $\mathbf{u}$ the displacement vector.

For optical forces, we use a spring foundation condition ($\mathbf{F} = -C_o \mathbf{u}$) by applying the calculated optical stiffnesses at the center of mass, represented by C_{Ox}, C_{Oy}, and C_{Oz}. We then compute the phononic dispersion relation in the first irreducible Brillouin zone (ΓX), where $\Gamma = (0,0,0)$ and $X = (\pi/a, 0, 0)$, assuming that the cells are repeated periodically along the x-direction presenting beam symmetry. We apply Floquet-Bloch boundary conditions along the x-direction in the unit cell:

$$\mathbf{u}(x + a, y, z) = \mathbf{u}(x, y, z) e^{jk_x a}, \quad \text{(C5)}$$

with $\mathbf{k} = (k_x, 0, 0)$ the reduced Bloch wavevector and $\mathbf{u}(x, y, z)$ the displacement vector.